RSC Advances

PAPER

View Article Online
View Journal | View Issue

Cite this: *RSC Adv.*, 2017, **7**, 15211

Deoxygenation of coal bed methane on $LaCoO_3$ perovskite catalyst: the structure evolution and catalytic performance

Zhenyang Zhao,† Li Wang,† Jian Ma, Yafen Feng, Xiaoming Cao, Wangcheng Zhan, Yanglong Guo, Yun Guo* and Guanzhong Lu

A series of perovskite-type $LaBO_3$ (B = Fe, Co, Mn, and Ni) materials have been studied as catalysts for coal bed methane (CBM) deoxygenation. Among them, $LaCoO_3$ shows the best catalytic performance and stability, O_2 could be completely eliminated by CH_4 to produce CO_2 and H_2O in the range of 400–720 °C, and the complete deoxidization could be maintained at temperatures of 400, 500, 600, and 660 °C for 100 h. Furthermore, the structure of $LaCoO_3$ could transform from perovskite to Co/La_2O_3 through $La_2CoO_4/LaCoO_3$ and La_2CoO_4/Co_3O_4 during the process of CBM deoxygenation. The results of H_2-TPR and O_2-TPO showed the perovskite $LaCoO_3$ is like a smart catalyst, whereby the Co species could reversibly move into and out of the perovskite structure depending on the temperature and reaction atmosphere. When Co species exist in an oxidised state (Co_3O_4, La_2CoO_4 and/or $LaCoO_3$), the CH_4 in CBM is completely oxidized by O_2 to produce CO_2 and H_2O, the results of isotopic tracer experiments and pulse reaction demonstrate that the reaction follows the Mars–van Krevelen mechanism. However, the preferred products of the CBM deoxygenation reaction are CO and H_2 on Co/La_2O_3 through partial oxidation of CH_4. With the structure transforming from Co/La_2O_3 to $LaCoO_3$ after reoxidation by O_2, the activity of CBM deoxygenation could be recovered.

Received 17th December 2016
Accepted 13th February 2017

DOI: 10.1039/c6ra28339j

rsc.li/rsc-advances

1. Introduction

Coal bed methane (CBM), also known as coal mine gas, is a kind of flammable gas whose main component is methane.[1] The direct emission of CBM is not only a waste of energy, but also pollutes the environment, because the warming potential of CH_4 is over 20 times of CO_2 as a greenhouse gas.[2] At a typical gassy mine, CBM is mainly emitted in three streams: (1) gas drained from the steam before mining, containing 60–95 vol% CH_4 and inert gas, which could be directly used or easily used to produce pure CH_4; (2) gas drained from the worked areas of the mine, *e.g.* goaf, containing 30–95 vol% CH_4 and some O_2 (2–6 vol%);[3,4] (3) CH_4 ventilation air (0.1–1 vol% CH_4).[5]

For the utilization of CBM with high CH_4 concentration and low O_2 concentration, it is necessary to remove the O_2 from the mixture, because the existence of O_2 could be dangerous in the process of storage and transportation. Usually, two main methods are used in CBM deoxygenation: non-catalytic and catalytic deoxidization. The common non-catalytic methods include the adsorption of O_2, coke burning and deep freezing methods.[6–8] Compared with non-catalytic methods, the catalytic deoxygenation of CBM is a convenient and effective method to eliminate O_2 by catalytic combustion of CH_4.[9–11] However, the catalytic combustion of CH_4 is a violent exothermal reaction with a huge ΔH_{298} of -802.7 kJ mol^{-1}, which could induce a severe temperature runaway of the reactor and sintering of the catalyst. Meanwhile, the high reaction temperature could cause CH_4 partial oxidation and a reforming reaction to produce CO and H_2 under the conditions of a large excess of CH_4.[12–14] Therefore, a desirable catalyst used in catalytic deoxygenation of CBM should not only have high activity to remove O_2 at low temperatures, but also avoid the production of H_2 and CO through side reactions (partial oxidation, cracking and/or reforming reaction) across a wide temperature range.

Furthermore, the composition of the reaction gas in the CBM deoxidization reaction varies from aerobic conditions to reducing conditions with the consumption of O_2, which requires the catalyst to maintain high performance under oxidizing and reducing conditions simultaneously. It is another challenge for the deoxygenation catalyst.

Supported noble metal catalysts are widely used in the catalytic combustion of CH_4.[15–20] However, the excess CH_4 in the reaction gas would lead to particle oxidation or cracking reactions, and produce H_2 and CO at temperatures as low as 400 °C while providing high CH_4 conversion.[21–26] Lyubovsky *et al.*[27] prepared Al_2O_3-supported Pd, Pt and Ru catalysts for CH_4

Key Laboratory for Advanced Materials and Research Institute of Industrial Catalysis, School of Chemistry & Molecular Engineering, East China University of Science and Technology, Shanghai 200237, People's Republic of China. E-mail: yunguo@ecust.edu.cn; Fax: +86 21 64253703; Tel: +86 21 64253703

† These authors contributed equally to this work.

oxidation under both fuel-rich and fuel-lean conditions. The partial oxidation products of H_2 and CO appeared under fuel-rich conditions above the light-off temperature, and their concentration increased with increasing temperature. In addition, the chemical state change of the noble metal in the process of CBM deoxygenation could affect the activity of catalyst. Lu *et al.*[28–30] reported CBM deoxygenation on Pd–PdO–NiO/Ni-foam and found the oscillation of O_2 conversion to be due to the formation of inert metal Pd under the reducing conditions. The presence of PdNi (alloy) induced by the *in situ* reaction could eliminate this O_2 oscillation, and O_2 completely oxidized CH_4 to CO_2 and H_2O in the temperature range of 350–500 °C.

Compared with the supported noble metal catalysts, transition metal oxide catalysts (such as Cu, Co Ni *etc.*) also have attracted great attention.[31–33] For example, Tao *et al.*[34] prepared a nano-$NiCo_2O_4$ catalyst *via* a co-precipitation method, which showed high activity for CH_4 combustion under conditions of excess O_2 in the temperature range of 350–550 °C due to the integration of nickel cations, cobalt cations and surface lattice oxygen atoms/oxygen vacancies at the atomic scale.

The perovskite-type oxides (ABO_3) have high temperature stability in hydrocarbon (C_nH_{2n+2}) oxidation[35,36] and reforming reactions.[37,38] For example, $LaCoO_3$ and partially substituted $LaCoO_3$ have been confirmed to have high activities and stabilities for the partial oxidation of CH_4.[39–41] Generally, perovskites prepared with La in the A position, and Co, Mn, Fe or Ni in position B, are used in the catalytic combustion of CH_4.[42–45] Meanwhile, the temperature of partial oxidation or reforming of CH_4 over perovskite catalyst usually exceeds 600 °C, which is much higher than that of supported noble metal catalysts and the transition metal oxide catalysts.[46,47] For example, Slagtern and Olsbye[48] studied the partial oxidation of CH_4 to syngas at 800 °C on La–M–O (M = Co, Ni, Rh, and Cr) perovskite catalysts, and found the main product was CO_2 on La–Co–O with the main phase of $LaCoO_3$, Co_3O_4, and La_2O_3.

Furthermore, the structure of perovskite-type oxides could be reversibly changed depending on the composition of the reaction atmosphere. Nishihata *et al.*[49] reported that $LaFe_{0.57}Co_{0.38}Pd_{0.05}O_3$ exhibited high catalytic activity during long term ageing, and the Pd reversibly moved into and out of the perovskite lattice during the cycle between oxidative and reductive atmospheres. Hence, the perovskite type catalyst may be a good candidate as a catalyst for CBM deoxygenation, and may be able to remove O_2 from the CBM *via* CH_4 combustion at a relatively low temperature, and maintain total oxidation across a wide temperature range by prohibiting partial oxidation and other side reactions.

In this work, perovskite-type oxides $LaBO_3$ (B = Co, Mn, Fe and Ni) were prepared, and the activity and stability of $LaBO_3$ for CBM catalytic deoxygenation were investigated. The evolution of $LaCoO_3$ perovskite structure in the reaction and reaction mechanism were also explored.

2. Experimental section

2.1 Catalyst preparation

The perovskite-type oxides ($LaBO_3$, B = Co, Mn, Fe and Ni) were prepared by the co-precipitation method. A stoichiometric amount of metal nitrate mixture solution and sodium hydroxide solution were simultaneously dropped into a NaOH solution with pH of 9–10 under stirring at 60 °C. The pH value of the mixture solution was kept in the range of 9–10 during the whole precipitation process. The obtained precipitate was aged at 60 °C for 2 h. After being washed by deionized water to neutral pH, the precipitate was filtered and dried at 100 °C for 12 h then calcined in air at 750 °C for 3 h to obtain the $LaBO_3$ catalysts. The BET surface areas of the prepared $LaBO_3$ are in the range of 12 to 15 $m^2\ g^{-1}$.

2.2 Catalyst characterization

The powder X-ray diffraction patterns (XRD) of catalysts were obtained with a RigakuD/max 2550 VB/PC diffractometer with a Cu Kα radiation ($\lambda = 1.54056$, scanning step 0.02°). Spectra were collected in a range of $2\theta = 10$–80° with a scanning rate of 6° min^{-1}. In order to obtain more details about the structure of the sample after reduction, the mapping of the elements was measured on the JOEL 2100 instrument operating at 200 kV.

The X-ray photoelectron spectroscopy (XPS) spectra were recorded on an AXIS-Ultra-DLD spectrometer with a Al Kα X-ray source (1486.6 eV). The base pressure inside the analysis chamber was 3×10^{-10} Torr. The XPS spectra of the selected elements were measured with the constant analyzer pass energy of 40 eV. All binding energies (BE) were referenced to the adventitious C 1s peak (BE = 284.8 eV).

The specific surface areas of the catalysts were measured using the N_2 adsorption isotherm at −196 °C by using an automatic Micromeritics ASAP 2020 analyzer.

The temperature-programmed reduction of H_2 (H_2-TPR) experiments were carried out by a conventional flow system equipped with a thermal conductivity detector (TCD). 100 mg catalyst was calcined at 400 °C for 1 h in air before the TPR reaction, and then cooled to room temperature. The pretreated catalyst was heated in a flow of 5 vol% H_2/N_2 (45 mL min^{-1}) at a heating rate of 10 °C min from room temperature to 800 °C. After H_2-TPR, the catalyst was maintained at 800 °C for 1 h in a flow of 5 vol% H_2/N_2 (45 mL min^{-1}), then purged with pure He for 1 h. After cooling to room temperature in a He flow, the temperature programmed oxidation of O_2 (O_2-TPO) was performed using the same apparatus; 1 vol% O_2/He (50 mL min^{-1}) was used in O_2-TPO, and the composition of the outlet gas was monitored by an on-line quadrupole mass spectrometer (IPC 400, INFICON Co. Ltd.).

Isotope tracer experiments were conducted in the quartz tube reactor and the effluent gas was monitored by an on-line quadrupole mass spectrometer (MS, IPC 400, INFICON Co. Ltd.).

The catalyst was pretreated at 700 °C for 2.5 h in pure He at 50 mL min^{-1}. 500 mg catalyst was used in the pulse experiments, 517.3 μL of 12 vol% $^{18}O_2$/6 vol% CH_4 was pulsed into the reactor 20 times. 200 mg catalyst was used in the continuous isotope tracer experiments at different designated temperatures, 12 vol% $^{18}O_2$/6 vol% CH_4 was used as the reaction gas.

The reaction orders of O_2 and CH_4 were measured in the temperature range of 340 to 410 °C with feed steams of 4.0–12.0

kPa O_2, CH_4 and N_2. 1.0 kPa CH_4 was used to investigate the catalytic combustion of CH_4, and 50.0 kPa CH_4 was used in the deoxidization of CBM. The O_2/CH_4 conversion was adjusted to below 15% by varying the space velocity in the range of 6000–72 000 mL g^{-1} h^{-1} so as to eliminate the thermal effect and diffusion effect.

CH_4 and O_2 pulse experiments were conducted on the same apparatus as that for the isotope tracer experiments. The procedures were as follows: (1) 10 vol% CH_4/He was pulsed into 500 mg catalyst 20 times (CH_4-1st); (2) 20 pulses of pure O_2 was passed through the catalyst bed; (3) step 1 was repeated again (CH_4-2nd). The pulse volume was 517.3 μL.

2.3 Evaluation of the catalytic performance

The catalytic activities of $LaBO_3$ (B = Co, Mn, Fe and Ni) catalysts for the simulated deoxygenation of CBM were tested in a fixed bed quartz tubular reactor at atmospheric pressure, 300 mg catalyst (40–60 mesh) diluted with 2 g silica sand (20–40 mesh) was used. The feed gas, containing 50 vol% CH_4, 6 vol% O_2 and N_2 to balance, was passed through the catalytic bed at a flow rate of 30 mL min^{-1}. The temperature of the catalyst bed was measured by a thermocouple inserted in the top of the catalyst bed, and the heating rate was 4 °C min^{-1}. An on-line gas chromatograph (Agilent 7890) was used to monitor the composition of the outlet gas. The catalyst activity was expressed by T_{10} and T_{90} of O_2, which corresponded to the reaction temperatures required for 10% and 90% O_2 conversion, respectively.

Because the excess CH_4 in the feed gas could lead to partial oxidation or the reforming reaction to produce CO and H_2 at high temperature, the temperature range between the lowest temperature of complete conversion (LTCC) of O_2 and the initial temperature of H_2 formation is defined as the operation window of the catalyst for the deoxygenation reaction.

3. Results

3.1 Catalytic activities of $LaBO_3$

The catalytic activities of $LaBO_3$ (B = Co, Fe, Mn and Ni) for CBM deoxygenation are shown in Fig. 1. The type of transition metal in the B-site shows a significant effect on the catalytic activity of the perovskites. $LaFeO_3$ shows the lowest activity for O_2 elimination, T_{10} and T_{90} are 350 and 450 °C, respectively. Meanwhile, $LaCoO_3$ exhibits the highest catalytic activity, the T_{10} and T_{90} are 300 and 390 °C, respectively. Combined with the results of the BET surface area in Table 1, the activity of the catalyst is not directly related to its surface area.

The excess CH_4 in the feed gas could produce H_2 and CO by the partial oxidation or reforming reaction at high reaction temperature (>700 °C). The production of H_2 following the reaction temperature in CBM deoxygenation on different catalysts is shown in Fig. 1b. CO was observed simultaneously but is not shown. The results in Fig. 1b show the initial sequence of H_2 formation is $LaFeO_3$ < $LaMnO_3$ < $LaNiO_3$ < $LaCoO_3$, and the H_2 formation on $LaNiO_3$ increases more rapidly than the others when the temperature exceeds 700 °C. Combined with the

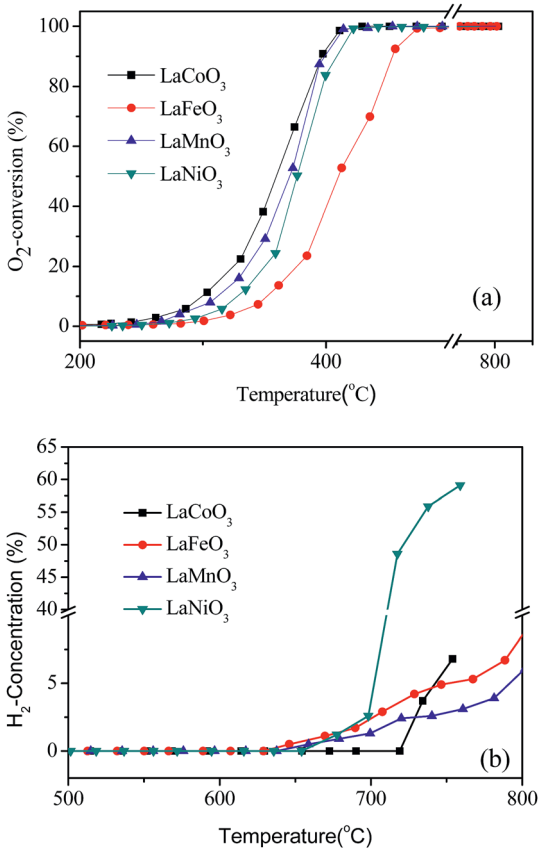

Fig. 1 The conversion of O_2 (a) and production of H_2 (b) in the deoxygenation reaction by $LaBO_3$ catalysts as a function of temperature.

results in Fig. 1a, $LaCoO_3$ shows the widest operation window, where O_2 could be completely eliminated by CH_4 in the temperature range of 400 to 720 °C. Continuously increasing the reaction temperature, the amount of H_2 and CO increased rapidly. Therefore, catalyst $LaCoO_3$ was selected for the further investigation in the following sections.

The stability of $LaCoO_3$ for deoxygenation reaction was investigated at temperatures of 360, 400, 500, 600, and 660 °C for 100 h. The results in Fig. 2 show O_2 conversion was maintained at 360 °C at about 75% for 100 h, and O_2 could be completely eliminated at 400 and 660 °C for 100 h, and H_2 and CO were not detected during the whole experiments. The same results were obtained at 500 and 600 °C, which are not shown. After reaction at 660 °C for 100 h, the light-off activity of the aged catalyst is nearly consistent with the fresh one (Fig. 2b), which indicates that $LaCoO_3$ has high stability for the deoxygenation reaction in the temperature range of 400–660 °C.

3.2 XRD

The XRD patterns of the fresh $LaBO_3$ catalysts are exhibited in Fig. 3. The prepared $LaBO_3$ (Ni, Mn and Co) show a typical hexagonal perovskite structure. For catalyst $LaFeO_3$, the major phase is orthorhombic perovskite structure, and some weak diffraction peaks corresponding to Fe_2O_3 and La_2O_3 are also

Table 1 The cell parameters[a], crystallite size[b] and BET area of the perovskites

	$LaCoO_3$	$LaFeO_3$	$LaMnO_3$	$LaNiO_3$
Spatial group	Hexagonal	Orthorhombic	Hexagonal	Hexagonal
a (Å)	5.4358	5.4672	6.0731	5.5953
b (Å)	5.4358	6.7968	6.0731	5.5953
c (Å)	13.0643	28.8799	13.4010	5.6679
Crystallite size (nm)	39.1	53.72	10.7	26.4
BET area ($m^2\ g^{-1}$)	11	16	22	14

[a] The cell parameters were obtained by Rietveld refinement calculations from the diffractogram of the structures. [b] The crystallite size was calculated by the Debye–Scherrer formula.

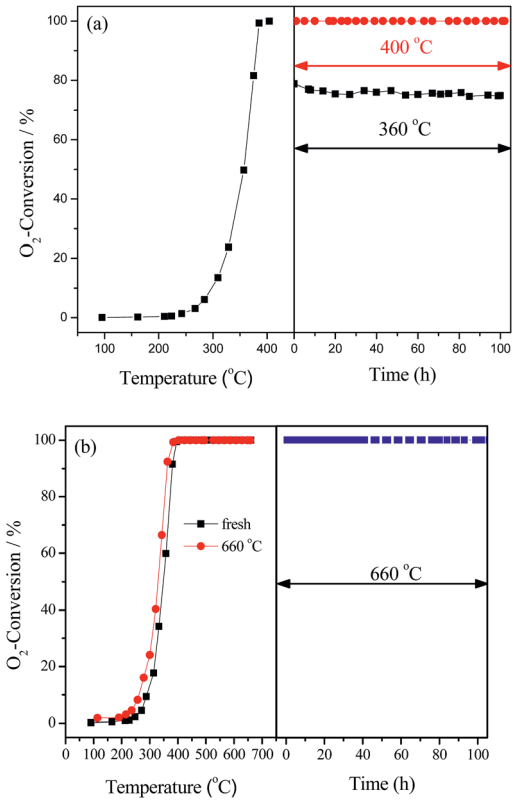

Fig. 2 The stability of $LaCoO_3$ measured at 360, 400 °C (a) and 660 °C (b). In part (b) the catalytic activity of fresh $LaCoO_3$ (■) and after reaction at 660 °C for 100 h (●) are compared.

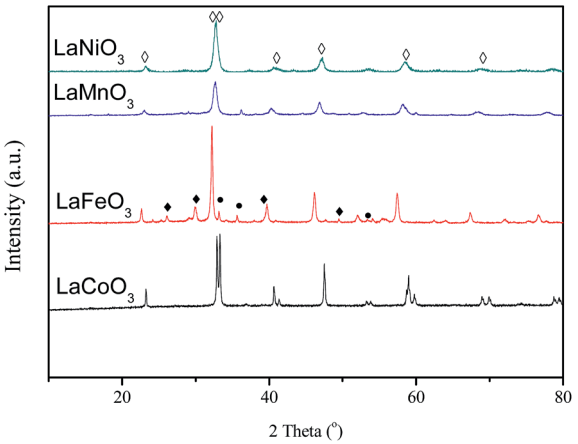

Fig. 3 XRD patterns of $LaBO_3$ (◇: perovskite; ●: Fe_2O_3; ◆: La_2O_3).

detected at $2\theta = 33$, 35, 49 and 54° and $2\theta = 26$, 30, 39 and 52°, respectively. The cell parameters, crystallite size and BET surface area of the perovskites are list in Table 1.

Fig. 4 shows the XRD patterns of $LaCoO_3$ after stability tests at different temperatures. Compared with the results in Fig. 3, there is no observable difference in the $LaCoO_3$ structure after reaction at 400 and 500 °C for 100 h (Fig. 4a and b), which indicates the stability of the perovskite structure. However, after reaction at 600 °C for 100 h (Fig. 4c), the structure of $LaCoO_3$ transforms from perovskite into a mixture of perovskite ($LaCoO_3$, 2θ = 23, 33, 40, 53 and 59°) and perovskite-like (La_2CoO_4, 2θ = 24, 32, 43, 47 and 65°). Continuously increasing the reaction temperature to 660 °C, only perovskite-like La_2CoO_4 and Co_3O_4 crystal phases are detected after 100 h reaction (Fig. 4d). Combined with the results in Fig. 2, it could be concluded that the structure change of $LaCoO_3$ is dependent on the reaction temperature, but this structure evolution does not bring an apparent difference in the catalytic performance of $LaCoO_3$ for CBM deoxygenation.

When the deoxygenation reaction is finished at 800 °C, the perovskite structure of $LaCoO_3$ is completely destroyed, and only La_2O_3 is detected at 26, 30, 39 and 52° (Fig. 4e). The results

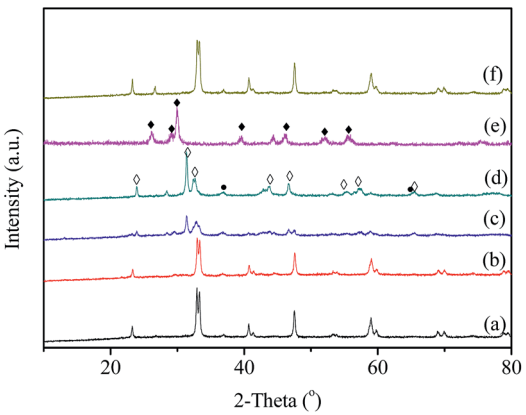

Fig. 4 The XRD patterns of the $LaCoO_3$ after reaction at 400 (a), 500 (b), 600 (c), and 660 °C (d) for 100 h and 800 °C (e), the re-oxidation of sample (e) at 750 °C in air (f) (◇: La_2CoO_4; ●: Co_3O_4; ◆: La_2O_3).

in Fig. 1 show the production of H_2 and CO when the reaction temperature was higher than 720 °C, which could lead to the reduction of $LaCoO_3$.[46] The diffraction peaks of Co species cannot be observed, which means Co species are highly dispersed or below the detection limit of XRD. However, it is worth noting that the completely destroyed $LaCoO_3$ could be reverted back to the perovskite structure after reoxidation at 750 °C in air (Fig. 4f).

3.3 XPS characterization

XPS characterization is performed to investigate the surface chemical state of the catalysts. Fig. 5 shows the Co 2p spectra of $LaCoO_3$ after reaction at different temperatures (400, 500, 600, and 660 °C) for 100 h. The resolution of the asymmetrical spectra of Co 2p shows the co-existence of two species at BE of 779.8 and 782.1 eV, which could be ascribable to Co^{3+} and Co^{2+}, respectively.[50,51]

The surface Co^{2+}/Co^{3+} ratio of $LaCoO_3$ after reaction is much higher than that of fresh catalyst, and the Co^{2+}/Co^{3+} ratio increases with the increase in the reaction temperature as shown in Table 2, which indicates the partial reduction of $LaCoO_3$ during the reaction, and coincides with the results of XRD shown in Fig. 4. The predominant crystal phase changes from perovskite to a mixture of La_2CoO_4 and Co_3O_4 through the mixed phase of $LaCoO_3$ and La_2CoO_4, the average chemical state of the surface Co species is gradually reduced during this process.

3.4 Temperature programmed reaction

In order to further investigate the effects of reaction gas and temperature on structure evolution of $LaCoO_3$ during the reaction, experiments of H_2-TPR and O_2-TPO are carried out.

The H_2-TPR profile of fresh $LaCoO_3$ shows three reduction peaks in Fig. 6a. The peaks in the temperature range of 200–500 °C correspond to the reduction of the oxygen adsorbed on the catalyst surface and reduction of Co^{3+} to Co^{2+}, the high temperature peak at 500–800 °C could be assigned to the reduction of Co^{2+} to Co.[46,52,53] The XRD pattern of Fig. 7a demonstrates that the perovskite structure of $LaCoO_3$ has been completely destroyed and converted to a mixture of metallic Co and La_2O_3 after H_2-TPR, which coincides with that of $LaCoO_3$ after reaction at 800 °C (Fig. 4).

Table 2 The surface oxygen content (%) and Co^{2+}/Co^{3+} ratio of $LaCoO_3$ obtained by XPS analysis

Sample[a]	Surface oxygen content (%)	Co^{2+}/Co^{3+}
Fresh	56.75	0.48
400 °C	53.72	0.83
500 °C	49.00	1.26
600 °C	49.23	3.29
660 °C	52.68	3.59

[a] After the stability test at specified temperature for 100 h.

After H_2-TPR, O_2-TPO of the reduced sample is performed. The result in Fig. 6b shows there are two O_2 consumption peaks: a significant peak is located at the range of 200–300 °C and a weak peak is observed at near 700 °C.

For the sample after H_2-TPR, XRD results show that the main phases are Co_3O_4 and La_2O_3 after reoxidation at 300 °C for 0.5 h (Fig. 7b), which indicates the O_2 consumption peak at range of 200–300 °C in Fig. 6b should correspond to the oxidation of metal Co to Co_3O_4 ($Co/La_2O_3 + O_2 \rightarrow Co_3O_4 + La_2O_3$). Because the oxidation of metal Co is a strong exothermic reaction, the accumulated heat could result in the direct oxidation of some metallic Co species to Co^{3+}. When the oxidation temperature is increased to 750 °C, the perovskite structure of $LaCoO_3$ was recovered ($Co_3O_4 + La_2O_3 + O_2 \rightarrow LaCoO_3$), the main phase of

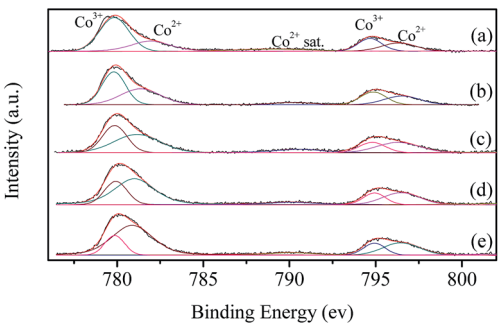

Fig. 5 XPS spectra of fresh $LaCoO_3$ (a) and aged $LaCoO_3$ after stability tests at temperatures of 400 (b), 500 (c), 600 (d) and 660 °C (e) for 100 h.

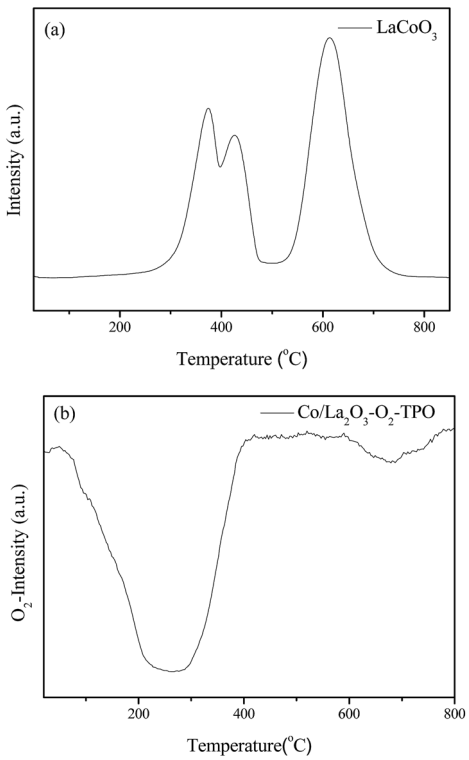

Fig. 6 H_2-TPR (a) and O_2-TPO (b) profiles of $LaCoO_3$.

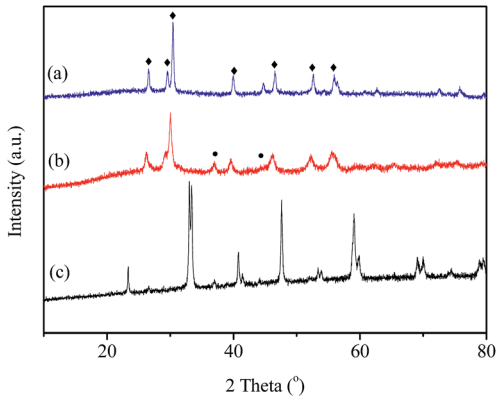

Fig. 7 (a) XRD patterns of $LaCoO_3$ reduced by H_2 at 800 °C (a); reoxidation by O_2 at 300 °C (b) and 750 °C (c). ●, Co_3O_4; ◆, La_2O_3.

the sample is perovskite with a minor Co_3O_4 phase observed at $2\theta = 37°$ (Fig. 7c), which corresponds to the O_2 consumption at the high temperature range in Fig. 6b.

3.5 Kinetic analysis

Fig. 8 shows the pressure-dependent reaction rates on the partial pressure of O_2 (P_{O_2}) from 4.0 to 12.0 kPa while keeping the partial pressure of CH_4 (P_{CH_4}) at 1.0 o 50.0 kPa, which corresponds to the catalytic combustion of CH_4 and deoxidization of CBM, respectively.

Under O_2 rich conditions, the O_2 reaction rate doesn't change with an increase in P_{O_2}, yielding an order of 0 with respect to O_2 at 420 °C. The fact that reaction order of O_2 is about zero shows the O_2 concentration hardly affect the rate of O_2 consumption, which implies the activation of CH_4 is the rate determination step for CH_4 combustion under O_2 excess.[54,55]

However, under oxygen lean conditions, the O_2 reaction rates increases with an increase in P_{O_2}, yielding an order of 0.25 with respect to O_2 at 370 °C, which demonstrates that the activation of O_2 is a key factor for CBM deoxygenation reaction. The apparent activation energy (E_a) of deoxygenation reaction on $LaCoO_3$ is 121 kJ mol^{-1}, as shown in Fig. 9.

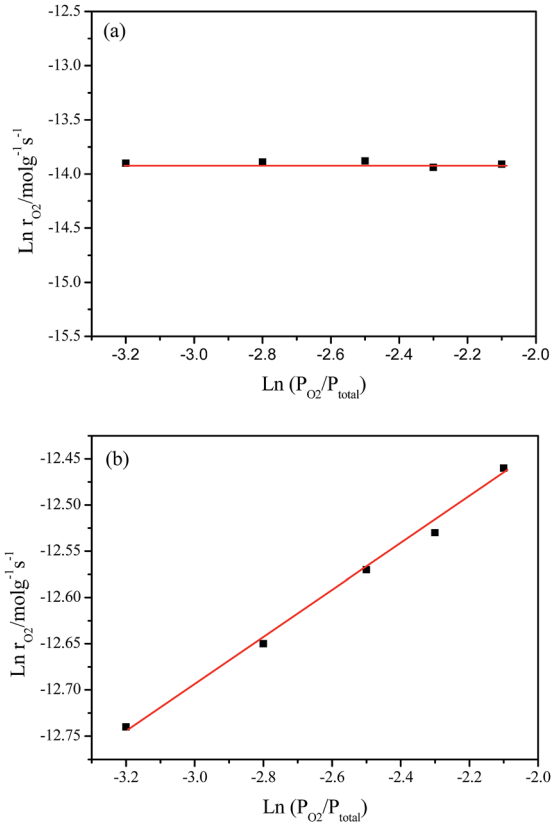

Fig. 8 ln r_{O_2} as a function of ln P_{O_2} over $LaCoO_3$: (a) at 420 °C, the feed gas consisted of 4–12% O_2 and 1% CH_4 at a space velocity of 30 000 mL g^{-1} h^{-1}; (b) at 370 °C, the feed gas consisted of 4–12% O_2 and 50% CH_4 at a space velocity of 48 000 mL g^{-1} h^{-1}.

3.6 Isotopic tracer experiments

The isotopic tracer pulse reaction results of $^{18}O_2$ + CH_4 are shown in Fig. 10. When the temperature is 600 °C, $^{18}O_2$ (O_2-36) is completely consumed in the 20 pulses on the $LaCoO_3$ (Fig. 10a), and the production of $C^{16}O_2$ (m/z = 44) could be observed at the same time. Furthermore, any CO_2 containing ^{18}O (m/z = 46 and 48) are not detected, which indicates CH_4 reacts with the lattice oxygen rather than gas $^{18}O_2$. The same results are obtained at the temperature of 700 °C (Fig. 10b).

When the feed gas of 12 vol% $^{18}O_2$/6 vol% CH_4 continuously passes through the catalyst bed at 600 °C, the result in Fig. 11a shows that $C^{16}O_2$ is produced immediately and exists as the dominant product in the first 300 s, then the content of $C^{16}O_2$ obviously decreases with the increase of reaction time. Meanwhile, the content of $C^{16}O^{18}O$ (46) and $C^{18}O_2$ (48) increases gradually. After 40 min, $C^{18}O_2$ becomes the main product, next is $C^{16}O^{18}O$. Similar results are obtained at 700 °C, as shown in Fig. 11b. Combined with the results in Fig. 10, it may be suggested that the deoxidization reaction of CBM may follow the Mars–van Krevelen mechanism: the CH_4 in the feed gas firstly reacts with lattice oxygen and creates oxygen vacancies, which could be replenished by the diffusion of lattice oxygen from bulk to surface and the adsorption and activation of gas O_2.

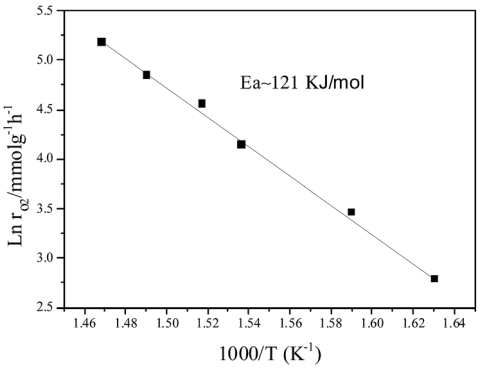

Fig. 9 Arrhenius plot of the reaction rate (ln r) *vs.* $1/T$ for O_2 deoxygenation over $LaCoO_3$.

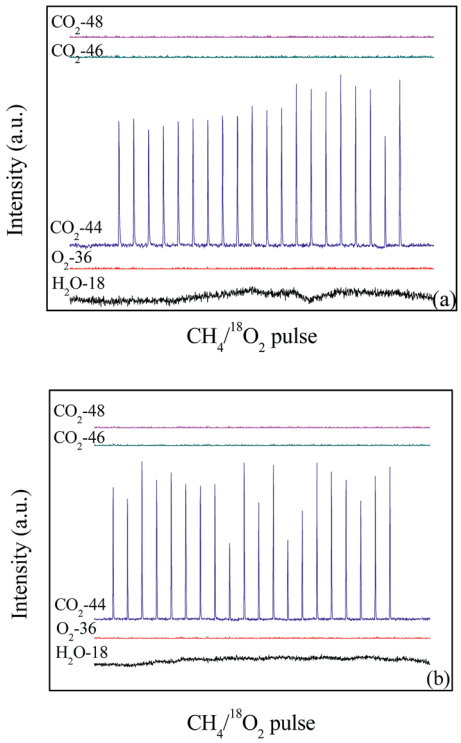

Fig. 10 The pulses test of catalyst $LaCoO_3$ under the conditions of 12 vol% $^{18}O_2$/6 vol% CH_4 at 600 (a) and 700 °C (b).

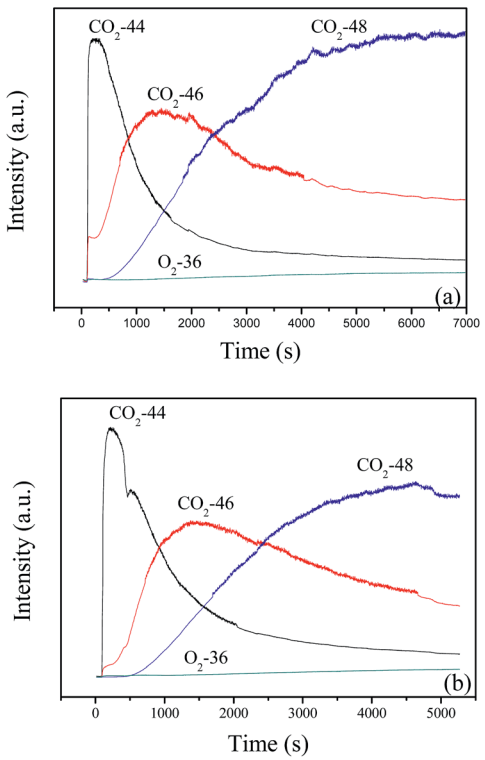

Fig. 11 The continuous reaction of 12 vol% $^{18}O_2$/6 vol% CH_4 balanced with N_2 on $LaCoO_3$ at 600 (a) and 700 °C (b).

3.7 Pulse reaction

The results in Fig. 4 showed structure transformation of $LaCoO_3$ during the CBM deoxygenation reaction. Separated CH_4 and O_2 pulse reactions on $LaCoO_3$ and pre-reduced $LaCoO_3$ at different temperatures are performed to explore the effects of $LaCoO_3$ structure on the CBM deoxygenation reaction and the formation mechanism of byproducts (H_2 and CO); the results are shown in Fig. 12 and 13.

For the CH_4 pulse reaction on $LaCoO_3$ at 700 °C (CH_4-1st, Fig. 12a), most of the CH_4 is consumed in 20 pulses, accompanied by the production of CO_2 and H_2O simultaneously. At the same time, weak signals of CO ($m/z = 28$) are also detected. Based on the standard spectra of CO_2, the CO signals may be induced by dissociative ionisation of CO_2 in the chamber of mass spectrometer. After the CH_4 pulses, 20 pulses of O_2 were passed through catalyst bed, CO_2/CO and H_2O were not detected during this process (not shown).

For the second run of CH_4 pulse reactions (CH_4-2nd, Fig. 12b), the similar results to those in CH_4-1st are obtained, which indicates CH_4 is oxidized by the lattice and/or adsorbed oxygen on $LaCoO_3$ to produce CO_2 and H_2O, but insufficient lattice oxygen or limited diffusion rate of lattice oxygen from bulk to surface leads to the residual CH_4.

The signals of CO ($m/z = 28$) in the pulse reaction are induced by the dissociative ionisation of CO_2 in the chamber of mass spectrometer, while not from the reaction production. We have already explained this phenomenon in the CH_4 pulse reaction on $LaCoO_3$ at 700 °C. However, the results in Fig. 1 show the production of CO and H_2 in the deoxidization reaction when the temperature is higher than 720 °C. It should be noted that the structure of the perovskite $LaCoO_3$ transforms to Co/La_2O_3 in the deoxidization reaction at a temperature higher than 720 °C (Fig. 4).

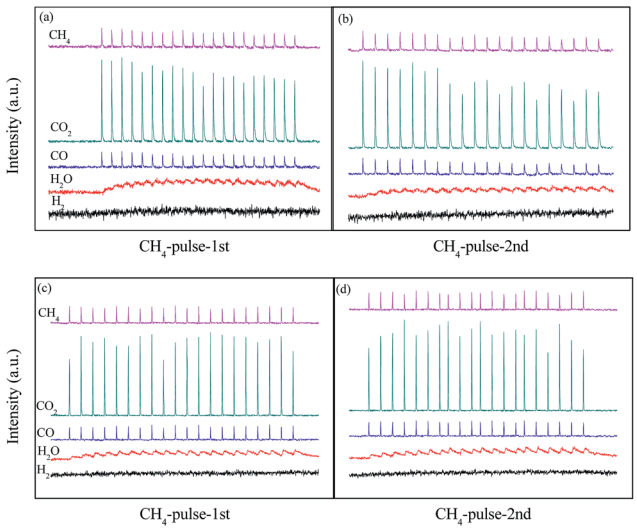

Fig. 12 CH_4 pulse reaction at 700 (a, b) and 800 °C (c, d) on $LaCoO_3$ (a and c are the first run of CH_4 pulse reaction, b and d are the second run).

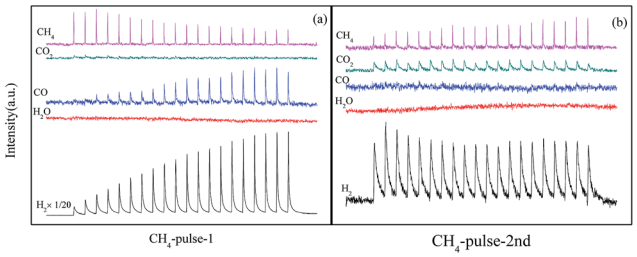

Fig. 13 CH_4 pulse reaction on Co/La_2O_3 at 700 °C (a: first run, b: second run).

In order to further investigate CBM deoxygenation reaction on Co/La_2O_3, the $LaCoO_3$ with perovskite structure is pretreated with 10% H_2/N_2 at 800 °C to obtain Co/La_2O_3 (Fig. 7), then the pulse reactions are performed after purging with He for 0.5 h. In the first run of CH_4 pulse reaction on Co/La_2O_3 at 700 °C (Fig. 13a), most of the CH_4 is consumed while H_2 and CO is generated, and the amount of H_2 and CO significantly increases with an increase in the number of pulses. Meanwhile, a trace amount of CO_2 is detected at the beginning of the pulse reaction, and the amount of CO_2 decreases gradually. After 3 pulses, the CO_2 could hardly be detected.

During the following O_2 pulse reaction, O_2 is completely consumed in the 20 pulses due to the oxidation of Co/La_2O_3. CO/CO_2, H_2 and H_2O are not observed during this process, the results are not shown.

After the O_2 pulse reaction, the second run of the CH_4 pulse reaction (CH_4-2nd) is performed. Fig. 13b shows the production of CO_2, CO and H_2, and their amount remains nearly constant during the 20 pulses, which is significantly different from the results in Fig. 13a. It may be induced by the partial Co/La_2O_3 oxidation to CoO_x/La_2O_3 by O_2 during the process of the O_2 pulse reaction. The formation of CoO_x/La_2O_3 decreases the amount of Co/La_2O_3, which leads to the significant decrease of CO and H_2.

4. Discussion

The results in Fig. 1 and 2 show $LaCoO_3$ behaves with high activity and stability for CBM deoxygenation across a wide temperature range, O_2 could be completely eliminated by CH_4 to produce CO_2 and H_2O in the range of 400–720 °C, and the activity of $LaCoO_3$ could be maintained after reaction at 400, 500, 600 or 660 °C for 100 h.

Roseno *et al.*[39] investigated the structure change of $LaCoO_3$ in partial oxidation of CH_4, and found that high temperature reduction could decompose the perovskite structure of $LaCoO_3$ to Co/La_2O_3, and metallic Co was oxidized to CoO in O_2, and further reacted with La_2O_3 to form La_2CoO_4 with spinel structure. During CBM deoxidization reaction, the structure of $LaCoO_3$ gradually transfers from perovskite to Co/La_2O_3 depending on the reaction temperature (Fig. 4). The H_2-TPR also showed the structure evolution of $LaCoO_3$ induced by the reduction of H_2 in the feed gas. Meanwhile, the destructed perovskite structure could be recovered from Co/La_2O_3 by calcination or reoxidation (Fig. 4 and 7). The structure evolution of $LaCoO_3$ depending on the temperature and reaction gas is shown schematically in Fig. 14, which demonstrates that Co species could reversibly move into and out of the perovskite structure depending on the temperature and reaction atmosphere.

Based on the results in Fig. 7, the $LaCoO_3$ has been reduced by 5 vol% H_2/N_2 (45 mL min^{-1}) at 750 °C for 30 min to obtain Co/La_2O_3 ($LaCoO_3$-R), then Co/La_2O_3 is reoxidized to perovskite $LaCoO_3$ ($LaCoO_3$-R-O). The activities of CBM deoxygenation in Fig. 15 show that $LaCoO_3$-R behaves with much higher activity than $LaCoO_3$-R-O, and there are no by-products of CO and H_2 before 720 °C, as with $LaCoO_3$-R-O. Compared with the result in Fig. 1, $LaCoO_3$-R-O shows nearly the same activity as fresh $LaCoO_3$. Combined with the results in Fig. 6 and 7, the apparently enhanced activity of $LaCoO_3$-R in the low temperature range may be derived from the oxidation of metallic Co by O_2. The above results indicate that even if the structure of $LaCoO_3$ with perovskite is completely destroyed when the CBM deoxygenation temperature exceeds 720 °C, the structure and activity could be recovered after calcination at 750 °C in O_2. Therefore, $LaCoO_3$ like a smart catalyst, its structure could be reversibly transformed between Co/La_2O_3, La_2CoO_4 and $LaCoO_3$ depending on the temperature and reaction atmosphere. This reversible structure evolution of $LaCoO_3$ could meet the challenge of the shift between oxidative and reductive atmosphere typically encountered in CBM deoxygenation.[49,56,57]

CH_4 combustion over metal oxides catalysts is known to follow a redox mechanism, and a variety of kinetic models for the catalytic combustion of methane, such as the Eley–Rideal, Langmuir–Hinshelwood or Mas–van Krevelen mechanism.[58,59] The results of isotopic tracer experiments in Fig. 10 and 11 confirms the deoxidization reaction of CBM on $LaCoO_3$ following the Mas–van Krevelen mechanism: the lattice oxygen reacts with CH_4 to produce CO_2, H_2O and oxygen vacancies, and the surface vacancies could be replenished by bulk lattice oxygen and gas O_2, which indicates the activation of O_2 should be a key factor for CBM deoxygenation reaction. The kinetic data in Fig. 8 also confirmed this. As shown in Fig. 14, $LaCoO_3$ could continuously provide lattice oxygen, accompanying the reduction of perovskite structure to Co/La_2O_3; meanwhile, O_2 gas could be adsorbed and dissociated on the surface, and

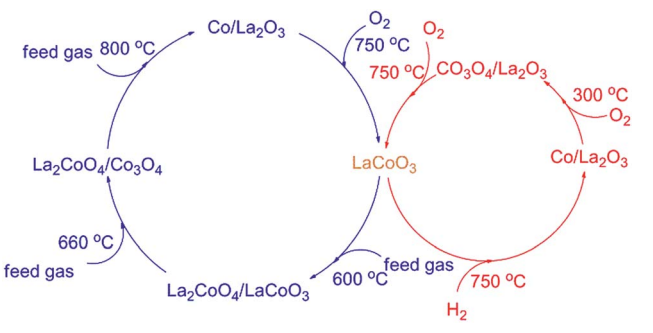

Fig. 14 The structure evolution of $LaCoO_3$ depending on the reaction gas and temperature.

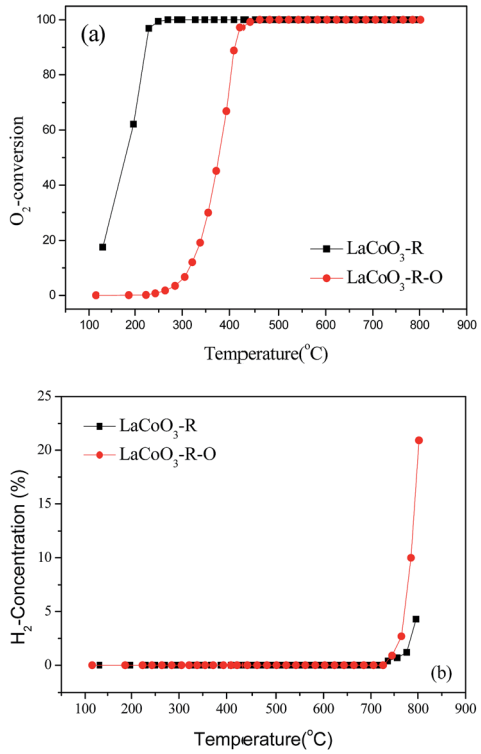

Fig. 15 The conversion of O_2 (a) and production of H_2 (b) over pre-treated $LaCoO_3$ under different conditions.

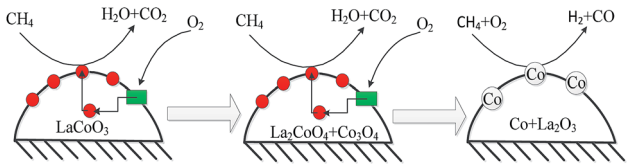

Fig. 16 CBM deoxygenation reaction on the $LaCoO_3$ catalyst (●: lattice oxygen; ■: oxygen vacancy).

incorporated into the lattice of the crystal as O^{2-} species.[60,61] And therefore, the perovskite $LaCoO_3$ acted as an oxygen pump toward CBM deoxidization reaction.[62]

The results in Fig. 1 show the O_2 could be completely eliminated by CH_4 in the temperature range of 400 to 720 °C. As shown in Fig. 14, $LaCoO_3$ could exist as perovskite, La_2CoO_4/Co_3O_4 and La_2CoO_4/$LaCoO_3$ in this temperature range, which indicates that the total oxidation of CH_4 by O_2 will take place on the catalyst despite the structure transformation of $LaCoO_3$ from perovskite to La_2CoO_4/Co_3O_4.

When the reaction temperature exceeds 720 °C, the CO and H_2 begin to form and their amounts increase significantly with continuously increasing the temperature (Fig. 1). However, the CO and H_2 could not be observed during the CH_4 pulse reaction on $LaCoO_3$ even when reaction temperature is 800 °C; the CH_4 pulse reaction on reduced $LaCoO_3$ (Co/La_2O_3) only produces CO and H_2 at 700 °C (Fig. 13a). Meanwhile, when Co/La_2O_3 is partially oxidized to CoO_x/La_2O_3, the co-existence of CoO_x/La_2O_3 and Co/La_2O_3 results in the formation of CO_2 and a significant decrease of CO/H_2.

These results show the products of CBM deoxygenation reaction mainly depend on the structure of $LaCoO_3$. When the Co species exists in an oxidised state, such as perovskite, La_2CoO_4 or CoO_x/La_2O_3, the CBM deoxygenation only produces CO_2 and H_2O by the total oxidation of CH_4. If Co species exists as metal, such as Co/La_2O_3, the preferred reaction is partial oxidation of CH_4, which would lead to the formation of CO and H_2.

Therefore, the CBM deoxygenation reaction on $LaCoO_3$ at different temperatures is shown schematically in Fig. 16. When the reaction temperature is below 720 °C, CH_4 reacts with the lattice oxygen to generate CO_2 and H_2O despite the structure transformation from perovskite to the mixture of Co_3O_4 and La_2CoO_4. With further increasing the reaction temperature, the lattice oxygen will be depleted due to the limited amount of O_2 in the feed gas and the perovskite structure of $LaCoO_3$ will be completely destroyed. Then, the partial oxidation of CH_4 could take place on the surface of metallic Co to produce by-products of CO and H_2.

5. Conclusions

The catalyst $LaCoO_3$ prepared by the co-precipitation method exhibits high activity and catalytic stability for the CBM deoxidization reaction across a wide temperature range. The O_2 could be completely eliminated by CH_4 to produce CO_2 and H_2O in the range of 400–720 °C, and complete deoxidization could be maintained in the temperature range of 400–660 °C for 100 h.

The perovskite $LaCoO_3$ acts as a smart catalyst during the process of CMB deoxidization; the structure of $LaCoO_3$ gradually transforms from perovskite to Co/La_2O_3 through La_2CoO_4/$LaCoO_3$ and La_2CoO_4/Co_3O_4 with the increasing reaction temperature, and these different structures could be transformed into each other depending on the reaction temperature and reaction gas.

When Co species exists as Co_3O_4, La_2CoO_4 and/or $LaCoO_3$, CH_4 is completely oxidized by O_2 to produce CO_2 and H_2O. The deoxidization of CBM on catalysts follows the Mars–van Krevelen mechanism, and the activation of O_2 was a key factor in the deoxidization of CBM. When Co species exist as metal Co (Co/La_2O_3), the preferred reaction in CBM deoxygenation would be partial oxidation, which generates CO and H_2. However, the complete oxidation of CH_4 could be recovered with the structure transformation of Co/La_2O_3 to $LaCoO_3$ after reoxidation by O_2.

Acknowledgements

This project was supported financially by the National Key Research and Development Program of China (2016YFC0204300), the National High Technology Research and Development Program of China (2015AA034603), NSFC of China (21171055, 21333003, 21571061), the "Shu Guang" Project of the Shanghai Municipal Education Commission (12SG29), and the Commission of Science and Technology of Shanghai Municipality (15DZ1205305).

Notes and references

1 L. I. Guo-jun, *Procedia Earth Planet. Sci.*, 2009, **1**, 94–99.
2 M. N. Debbagh, C. S. M. d. Lecea and J. Pérez-Ramírez, *Appl. Catal., B*, 2007, **70**, 335–341.
3 A. Olajossy, A. Gawdzik, Z. Budner and J. Dula, *Chem. Eng. Res. Des.*, 2003, **81**, 474–482.
4 D. Zhong and P. Englezos, *Energy Fuels*, 2012, **26**, 2098–2106.
5 S. Su and J. Agnew, *Fuel*, 2006, **85**, 1201–1210.
6 X. Guo, J. Ren, C. Xie, J. Lin and Z. Li, *Energy Convers. Manage.*, 2015, **100**, 45–55.
7 J. Ren, C. Xie, J.-Y. Lin and Z. Li, *Process Saf. Environ. Prot.*, 2014, **92**, 896–902.
8 D. W. X. C. W. Peng, Y. Z. X. Z. Keda and D. Yiying, *Coal Conversion*, 2009, **4**, 021.
9 C. Ö. Karacan, F. A. Ruiz, M. Cotè and S. Phipps, *Int. J. Coal Geol.*, 2011, **86**, 121–156.
10 C. J. Bibler, J. S. Marshall and R. C. Pilcher, *Int. J. Coal Geol.*, 1998, **35**, 283–310.
11 T. Thielemann, B. Cramer and A. Schippers, *Org. Geochem.*, 2004, **35**, 1537–1549.
12 C. H. Bartholomew, *Appl. Catal., A*, 1993, **107**, 1–57.
13 C. H. Bartholomew, *Appl. Catal., A*, 2001, **212**, 17–60.
14 F. Yin, S. Ji, P. Wu, F. Zhao and C. Li, *J. Catal.*, 2008, **257**, 108–116.
15 D. Kim, S. Woo, J. Lee and O. B. Yang, *Catal. Lett.*, 2000, **70**, 35–41.
16 R. D. Waters, J. J. Weimer and J. E. Smith, *Catal. Lett.*, 1994, **30**, 181–188.
17 L. F. Liotta, G. Di Carlo, A. Longo, G. Pantaleo and A. M. Venezia, *Catal. Today*, 2008, **139**, 174–179.
18 A. Maione, F. André and P. Ruiz, *Appl. Catal., A*, 2007, **333**, 1–10.
19 T. V. Choudhary, S. Banerjee and V. R. Choudhary, *Appl. Catal., A*, 2002, **234**, 1–23.
20 M. Cargnello, J. J. Delgado Jaen, J. C. Hernandez Garrido, K. Bakhmutsky, T. Montini, J. J. Calvino Gamez, R. J. Gorte and P. Fornasiero, *Science*, 2012, **337**, 713–717.
21 A. E. York, T. Xiao and M. H. Green, *Top. Catal.*, 2003, **22**, 345–358.
22 Y. H. Hu and E. Ruckenstein, *Adv. Catal.*, 2004, **48**, 297–345.
23 S. Yang, J. N. Kondo, K. Hayashi, M. Hirano, K. Domen and H. Hosono, *Appl. Catal., A*, 2004, **277**, 239–246.
24 H. Y. Wang and E. Ruckenstein, *J. Catal.*, 2001, **199**, 309–317.
25 V. R. Choudhary, B. Prabhakar, A. M. Rajput and A. S. Mamman, *Fuel*, 1998, **77**, 1477–1481.
26 V. R. Choudhary, A. M. Rajput and V. H. Rane, *Catal. Lett.*, 1992, **16**, 269–272.
27 M. Lyubovsky, L. L. Smith, M. Castaldi, H. Karim, B. Nentwick, S. Etemad, R. LaPierre and W. C. Pfefferle, *Catal. Today*, 2003, **83**, 71–84.
28 Q. Zhang, X.-P. Wu, Y. Li, R. Chai, G. Zhao, C. Wang, X.-Q. Gong, Y. Liu and Y. Lu, *ACS Catal.*, 2016, **6**, 6236–6245.
29 Q. Zhang, Y. Li, R. Chai, G. Zhao, Y. Liu and Y. Lu, *Appl. Catal., B*, 2016, **187**, 38–248.
30 Q. Zhang, X.-P. Wu, G. Zhao, Y. Li, C. Wang, Y. Liu, X.-Q. Gong and Y. Lu, *Chem. Commun.*, 2015, **51**, 12613–12616.
31 D. Dissanayake, M. P. Rosynek, K. C. C. Kharas and J. H. Lunsford, *J. Catal.*, 1991, **132**, 117–127.
32 A. C. Ferreira, A. P. Gonçalves, T. A. Gasche, A. M. Ferraria, A. M. B. d. Rego, M. R. Correia, A. M. Bola and J. B. Branco, *J. Alloys Compd.*, 2010, **497**, 249–258.
33 B. Christian Enger, R. Lødeng and A. Holmen, *Appl. Catal., A*, 2008, **346**, 1–27.
34 F. F. Tao, J.-j. Shan, L. Nguyen, Z. Wang, S. Zhang, L. Zhang, Z. Wu, W. Huang, S. Zeng and P. Hu, *Nat. Commun.*, 2015, **6**, 7798.
35 A. J. Zarur and J. Y. Ying, *Nature*, 2000, **403**, 65–67.
36 L. Fabbrini, A. Kryukov, S. Cappelli, G. L. Chiarello, I. Rossetti, C. Oliva and L. Forni, *J. Catal.*, 2005, **232**, 247–256.
37 R. Pereñíguez, V. M. González-DelaCruz, J. P. Holgado and A. Caballero, *Appl. Catal., B*, 2010, **93**, 346–353.
38 A. G. Bhavani, W. Y. Kim and J. S. Lee, *ACS Catal.*, 2013, **3**, 1537–1544.
39 K. T. C. Roseno, R. Brackmann, M. A. da Silva and M. Schmal, *Int. J. Hydrogen Energy*, 2016, **41**(40), 18178–18192.
40 M. R. Goldwasser, M. E. Rivas, M. L. Lugo, E. Pietri, J. Pérez-Zurita, M. L. Cubeiro, A. Griboval-Constant and G. Leclercq, *Catal. Today*, 2005, **107–108**, 106–113.
41 R. M. Navarro, M. C. Alvarez-Galvan, J. A. Villoria, I. D. González-Jiménez, F. Rosa and J. L. G. Fierro, *Appl. Catal., B*, 2007, **73**, 247–258.
42 J. Li, L. Zhao and G. Z. Lu, *Ind. Eng. Chem. Res.*, 2008, **48**, 641–646.
43 L. Fabbrini, I. Rossetti and L. Forni, *Appl. Catal., B*, 2010, **93**, 346–353.
44 L. Marchetti and L. Forni, *Appl. Catal., B*, 1998, **15**, 179–187.
45 J. G. McCarty and H. Wise, *Catal. Today*, 1990, **8**, 231–248.
46 R. Lago, G. Bini, M. A. Peña and J. L. G. Fierro, *J. Catal.*, 1997, **167**, 198–209.
47 V. R. Choudhary, B. S. Uphade and A. A. Belhekar, *J. Catal.*, 1996, **163**, 312–318.
48 Å. Slagtern and U. Olsbye, *Appl. Catal., A*, 1994, **110**, 99–108.
49 Y. Nishihata, J. Mizuki, T. Akao, H. Tanaka, M. Uenishi, M. Kimura, T. Okamoto and N. Hamada, *Nature*, 2002, **418**, 164–167.
50 C. V. Schenck, J. G. Dillard and J. W. Murray, *J. Colloid Interface Sci.*, 1983, **95**, 398–409.
51 Z. Gao and R. Wang, *Appl. Catal., B*, 2010, **98**, 147–153.
52 B. Białobok, J. Trawczyński, W. Miśta and M. Zawadzki, *Appl. Catal., B*, 2007, **72**, 395–403.
53 J. A. Villoria, M. C. Alvarez-Galvan, S. M. Al-Zahrani, P. Palmisano, S. Specchia, V. Specchia, J. L. G. Fierro and R. M. Navarro, *Appl. Catal., B*, 2011, **105**, 276–288.
54 Y. Han, L. Chen, K. Ramesh, E. Widjaja, S. Chilukoti, I. Kesumawinatasurjami and J. Chen, *J. Catal.*, 2008, **253**, 261–268.
55 J. Xu, Y. Q. Deng, Y. Luo, W. Mao, X. J. Yang and Y. F. Han, *J. Catal.*, 2013, **300**, 225–234.

56 N. Guilhaume, S. D. Peter and M. Primet, *Appl. Catal., B*, 1996, **10**, 325–344.
57 H. Tanaka, I. Tan, M. Uenishi, M. Taniguchi, M. Kimura, Y. Nishihata and J. i. Mizuki, *J. Alloys Compd.*, 2006, **408–412**, 1071–1077.
58 N. Bahlawane, *Appl. Catal., B*, 2006, **67**, 168–176.
59 V. Belessi, A. Ladavos, G. Armatas and P. Pomonis, *Phys. Chem. Chem. Phys.*, 2001, **3**, 3856–3862.
60 S. Royer, H. Alamdari, D. Duprez and S. Kaliaguine, *Appl. Catal., B*, 2005, **58**, 273–288.
61 G. Saracco, G. Scibilia, A. Iannibello and G. Baldi, *Appl. Catal., B*, 1996, **8**, 229–244.
62 R. Hammami, S. B. Aïssa and H. Batis, *Appl. Catal., A*, 2009, **353**, 145–153.